THE JOURNAL OF PHYSICAL CHEMISTRY B

Article

pubs.acs.org/JPCB

Role of Specific Cations and Water Entropy on the Stability of Branched DNA Motif Structures[||]

Tod A. Pascal,*[,†] William A. Goddard, III,*[,†,‡] Prabal K. Maiti,[§] and Nagarajan Vaidehi[⊥]

[†]Materials and Process Simulation Center, California Institute of Technology, Pasadena, California 91125, United States

[‡]World Class University (WCU) Professor, Graduate School of EEWS, Korea Advanced Institute of Science and Technology, Daejeon, Korea

[§]Center for Condensed Matter Theory, Department of Physics, Indian Institute of Science, Bangalore, India 560012

[⊥]Division of Immunology, Beckman Research Institute of the City of Hope, Duarte, California 91010, United States

Supporting Information

ABSTRACT: DNA three-way junctions (TWJs) are important intermediates in various cellular processes and are the simplest of a family of branched nucleic acids being considered as scaffolds for biomolecular nanotechnology. Branched nucleic acids are stabilized by divalent cations such as Mg^{2+}, presumably due to condensation and neutralization of the negatively charged DNA backbone. However, electrostatic screening effects point to more complex solvation dynamics and a large role of interfacial waters in thermodynamic stability. Here, we report extensive computer simulations in explicit water and salt on a model TWJ and use free energy calculations to quantify the role of ionic character and strength on stability. We find that enthalpic stabilization of the first and second hydration shells by Mg^{2+} accounts for 1/3 and all of the free energy gain in 50% and pure $MgCl_2$ solutions, respectively. The more distorted DNA molecule is actually destabilized in pure $MgCl_2$ compared to pure NaCl. Notably, the first shell, interfacial waters have very low translational and rotational entropy (i.e., mobility) compared to the bulk, an entropic loss that is overcompensated by increased enthalpy from additional electrostatic interactions with Mg^{2+}. In contrast, the second hydration shell has anomalously high entropy as it is trapped between an immobile and bulklike layer. The nonmonotonic entropic signature and long-range perturbations of the hydration shells to Mg^{2+} may have implications in the molecular recognition of these motifs. For example, we find that low salt stabilizes the parallel configuration of the three-way junction, whereas at normal salt we find antiparallel configurations deduced from the NMR. We use the 2PT analysis to follow the thermodynamics of this transition and find that the free energy barrier is dominated by entropic effects that result from the decreased surface area of the antiparallel form which has a smaller number of low entropy waters in the first monolayer.

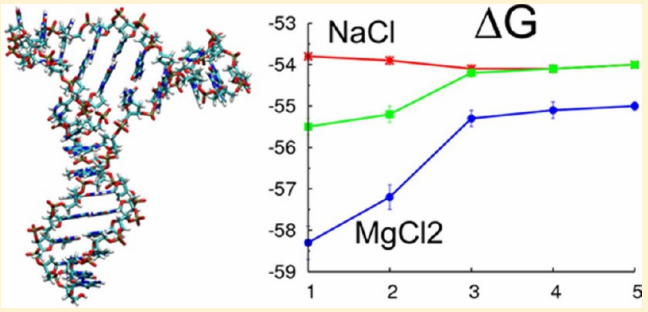

1. INTRODUCTION

The structure and function of branched nucleic acid motifs are varied and complex and critical to many cellular processes,[1] progression of degenerative diseases,[2,3] and serve as scaffolds for nanoscale machinery.[4,5] Three-way junctions (TWJs), the simplest members of this ubiquitous family, are prevalent during gene splicing and DNA recombination and replication.[6] Through branch migration (the stepwise exchange of base pairs between different arms of branched nucleic acids[7]), extended TWJs transition to more compact conformations, although this process requires the presence of divalent cations such as Mg^{2+}.[8,9] Here, one presumption is that Mg^{2+} more readily condenses on the negatively charged nucleic acid backbone than a monovalent ion like Na^{+}, thereby decreasing the electrostatic repulsion.[10]

The solvation environment around TWJs, and indeed all nucleic acids, contains both the neutralizing ions and interfacial water molecules. These interfacial waters serve the dual role of modulating the DNA−ion electrostatic interactions and must be carefully considered in accessing system thermodynamics.[11] Indeed, these interfacial waters may play a role in molecular recognition of the nucleic acids.[12,13]

Computational studies on the structure and stability of DNA using molecular dynamics (MD) based on validated interaction potentials or force fields have reported an A to B DNA transition[14] and produced a variety of crossover structures[15−17] showing good simulations agreement with experiments. However, simulations quantifying the free energy and entropic component of DNA stability are rare due to the enormous computational requirements of current methods based on

Received: June 30, 2012
Revised: September 20, 2012
Published: September 21, 2012

perturbation theory or umbrella sampling.[18] This limits our deeper understanding of the function of biomolecules in more complicated processes and our ability to employ rational design strategies for biomolecular nanotechnology.[17,19−21]

In this contribution we examine the influence of ions on the DNA structure and water thermodynamics by employing MD simulations and an efficient scheme of approximating the entropic and quantum effects of complex DNA solutions at the appropriate temperature and pressure.[22,23] We report here the application to the TWJ1[6] DNA three-way junction (Figure 1a)

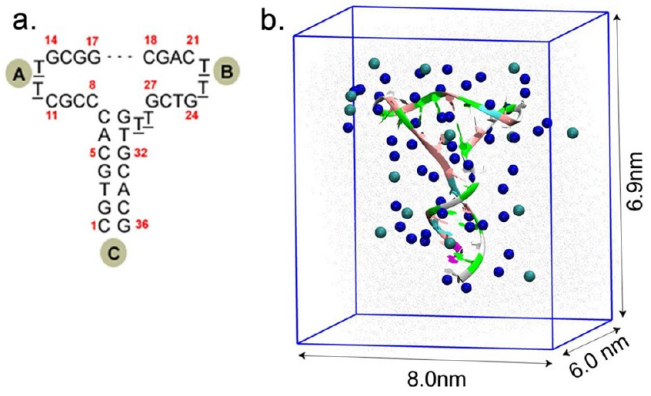

Figure 1. Description of TWJ1 structure. (a) Nucleotide sequence with unique arms (A, B, and C in the shaded circles) indicated. Base sequence numbers are indicated with red numbers next to the nucleotide. TWJ1 exists as an A/B stacked structure (i.e., arms A and B form a helix stacked on arm C) in monovalent salts or low concentration divalent salts. (b) Starting simulation cell configurations in our calculations. The cell is periodic in all three dimensions. Twenty-five Mg^{2+} (blue spheres) and 15 Cl^- (green spheres) ions were added to neutralize the DNA and provide 100 nM excess salt (assuming a 1.0 g/cm^3 water density) to match the experimental conditions. Note that, by this measure, the DNA concentration is 6.7 mM. The 8237 water molecules are not shown for presentation purposes.

since it is small (36 DNA nucleotides) and yet structurally sensitive to salt environments. Indeed, this family of TWJs is known to assume different stacked configurations in Mg^{2+} than in low Na^+ or in high Na^+ concentrations.[9,24,25] Such branch migration processes occur on the millisecond or second time scale, far outside the range of traditional MD simulations such as those employed here. However, we report here a transition from the stacking configuration of TWJ1 in high salt (an antiparallel conformation) to an opposite stacking configuration in low salt (a parallel conformation) that occurs over 100 ns.

In order to gain understanding about the thermodynamic driving forces and how they depend on the Na^+/Mg^{2+} ratio, we report here the thermodynamics of TWJ1 in explicit water at the physiological concentration of 0.1 M of either 100% (pure) NaCl, 50% NaCl/$MgCl_2$, or pure $MgCl_2$ by ionic strength. In addition, we report the case of a very low NaCl concentration. We analyze the total free energy and entropy arising from the DNA, ions, and various hydration shell waters separately. We also analyze the entropic effects by considering the translational and rotational entropy of the hydration shell. This analysis quantifies the forces controlling stability, allowing for interpretation of the observed structural changes along simple thermodynamic lines.

2. METHODS

2.1. Model Construction. The reported NMR structure (PDB code[26] 1EZN) consists of coordinates for 26 distance−geometry matches to the NMR data[6] which span a range of CRMS differences up to 3.5 Å. We took conformer 1 to be representative and inserted it into an orthorhombic, pre-equilibrated water box with initial cell dimensions of 81.1 × 69.3 × 60.1 Å^3 (Figure 1b). This procedure eliminated waters within 1 Å of the DNA structure. We then added ions to neutralize the DNA and an excess of either 100% NaCl, 50% NaCl/$MgCl_2$, or 100% $MgCl_2$ ions (Table 1) to achieve the 0.1

Table 1. Description of Systems Simulated in This Study[a]

	no. waters	no. Na^+	no. Mg^{2+}	no. Cl^-	no. atoms
100% NaCl	8327	50	0	15	26185
50% NaCl/MgCl2	8327	34	8	15	26177
100% MgCl2	8327	0	25	15	26158

[a]The water molecules were described using the SPC/E[29] water model, the DNA using the AMBER2010 force field,[28] Mg^{2+} ions using the Aqvist parameters,[30] and the Na^+ and Cl^- ions using the Joung and Cheatman[31] parameters.

M excess salt used in the experiments. When placing the counterions, we first calculated the solvated DNA electrostatic potential using the APBS[27] Poisson−Boltzmann solver and then replaced water molecules in the second solvation shell at regions of greatest electrostatic potential. The electrostatic potential was recalculated after every insertion.

2.2. Force Field and Simulation Parameters. The DNA molecule was described using the AMBER2010 force field,[28] while we choose the rigid SPC/E[29] force field for water. The magnesium parameters were taken from the work of Aqvist,[30] while the sodium and chlorine parameters were taken from the work of Joung and Cheatman,[31] shown to reproduce the experimental solvation free energy of ionic solutions (Table S1).

All simulations were performed using the LAMMPS[32] MD code. After initial energy minimization, each system was heated from 0 to 300 K over 1 ns using a Nose−Hoover thermostat with temperature relaxation constant of 0.1 ps. This was followed by annealing dynamics where the temperature of the ions and water were raised in 3 cycles to 600 K over 1 ns, while the DNA was kept rigid by means of a 100 kcal/mol harmonic spring. The annealing procedure allows for rapid equilibration of the ions and water[33] while maintaining DNA structural fidelity. Production constant-pressure, constant-temperature (or NPT) dynamics were then commenced for 50 ns at 1 atm and 300 K, with 0.1 and 2.0 ps temperature and pressure coupling constants, respectively. The short-range van der Waals interactions were smoothly splined to 0 between 13 and 15 Å using a seventh order taper function and the long-range electrostatics were evaluated using the PPPM[34] methods with a real space cutoff of 15 Å and a 10^{-5} error tolerance. The van der Waals interactions not explicitly defined in the force fields above were obtained using arithmetic combination rules as standard for the AMBER force field.

2.3. Structural Analysis. Snapshots of the system were saved every 1 ps of the 50 ns production dynamics and the coordinate root mean squared deviation (CRMSD) of the backbone atoms obtained using both the starting NMR structure and the equilibrated MD structures as reference. We accessed the size (end-to-end distance or radius of gyration—

dx.doi.org/10.1021/jp306473u | J. Phys. Chem. B 2012, 116, 12159−12167

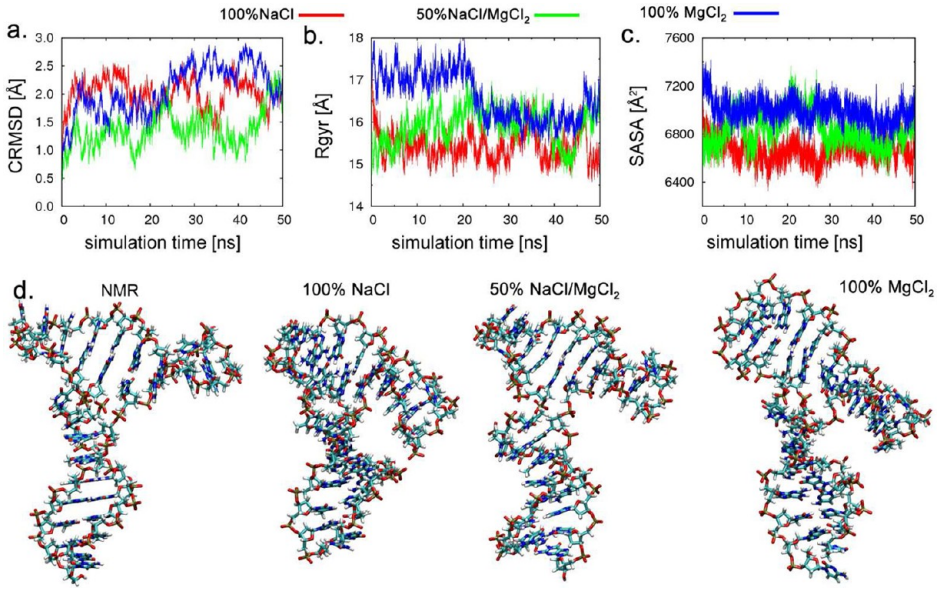

Figure 2. Time evolution of TWJ1 structural parameters. (a) Coordinate root mean squared deviation CRMSD of TWJ1 in $MgCl_2$ (red) and NaCl (blue), relative to the starting NMR structure. The CRMSD is determined using only the 14 central residues at the junction point (6–9, 16–19, 26–31) which gave unambiguous NMR NOE signals.[6] The converged MD structure differs from the starting NMR structure by 2.01 ± 0.27, 2.17 ± 0.51, and 2.41 ± 0.22 Å for the pure NaCl, 50% NaCl/$MgCl_2$, and pure $MgCl_2$ simulations, respectively, slightly larger than the 1.5 Å resolution from experiments and indicative that the MD procedure and force fields are accurate. The MD structures converge to within 1.75 Å of the average after 25 ns of dynamics, attesting to the precision of the force field. (b) Radius of gyration Rgyr of TWJ1. This provides a measure of the size of the DNA structure during dynamics. TWJ1 values in pure NaCl (15.4 ± 0.4 Å), 50% $MgCl_2$ (15.9 ± 0.4 Å), and pure $MgCl_2$ (16.1 ± 0.3 Å) are smaller than the starting NMR structure (18.2 Å). (c) Solvent-accessible surface area SASA of TWJ1. Our simulated structures in pure NaCl (6665 $Å^2$), 50% $MgCl_2$ (6800 $Å^2$), and pure $MgCl_2$ (6965 $Å^2$) are more compact than the NMR structure (7434 $Å^2$). (d) Snapshots of starting TWJ1 (NMR) structure, average structure after equilibration. TWJ1 in pure $MgCl_2$ shows significant distortions of the base-pair interactions.

Rgyr) of the DNA every 1 ps by calculating the largest principle moment of inertia. Similarly, the solvent-accessible surface area (SASA) was obtained by "rolling" a solvent molecule of probe radius 1.4 Å (representing a water molecule) around the TWJ1 surface.[35] DNA–water (oxygen atom) and DNA–ions distribution functions were obtained by binning the closest contact point to the DNA backbone (PO_4^{2-} unit).

2.4. Free Energy Analysis. After equilibration, we selected the last 250 snapshots (each 100 ps apart) and ran an additional 20 ps of dynamics in the microcanocical (NVE) ensemble, saving the atomic positions and velocities every 4 fs. Absolute molar entropies and zero-point energy corrections to the enthalpy[34] were obtained using the two-phase thermodynamics (2PT) method.[16] Details of the method are presented in the Supporting Information. Briefly, the partition function of the system, which contains all the information necessary to extract the relevant thermodynamic properties, is extracted from the total density of states (DOS). Practically, the DOS is the Fourier transform of the atomic velocity autocorrelation function. The DOS is then self-consistently partitioned into a hard-sphere (anharmonic) and a solid (harmonic) component, as first proposed by Eyring and Ree.[36] Using the appropriate quantum weighting functions, the total system thermodynamics can be recovered by a linear combination of the two DOS. The efficiency of the 2PT method means that the system thermodynamics are evaluated dynamically along the trajectory for typically only a 10–20% increase in total simulation time.

The 2PT method has been validated by calculating the thermodynamics of Lennard-Jones systems,[37] organic liquids,[38] carbon dioxide over the entire phase diagram,[39] and water from the vapor point to the critical point[22] with accuracy comparable to thermodynamic integration. It has been used in calculating the entropy of water in different domains of PAMAM dendrimers,[40] in determining various phases of dendrimer liquid crystals,[41] to investigate hydrophobic/hydrophilic hydration,[42] in accessing the stability of water molecules in hydrogels,[43] and in calculating the relative stability of various aggregates[44] and to show that water molecules in both grooves of DNA have significantly lower entropies than for bulk water.[45] More recently it has been used to uncover the entropic driving force for water filling of carbon nanotubes[46,47] and in determining the stability of hydrocarbons in near earth conditions.[48]

The water shell assignments were made by calculating the phosphate–water distribution functions, with waters assigned based on their average distance from the DNA surface during the 20 ps. Since 2PT only relies on atomic coordinates and velocities, this allowed us to consider the thermodynamics of the DNA, ions, and water shells separately.

3. RESULTS AND DISCUSSION

3.1. Structural Properties and Comparison to Experiments. After equilibration, we find that our average MD structures agree reasonably well with the starting NMR model, with a CRMS deviation of 2.5 ± 1.5 Å (Figures 2a and S2). There are some important differences, however, in the structures. First, the radii of gyration of our MD structures are 15.4, 15.9, and 16.1 Å for the pure NaCl, 50% NaCl, and pure $MgCl_2$ simulations, respectively (Figure 2b), which are 15%, 13%, and 11% smaller than the NMR structure. Similarly, we find solvent surface areas (Figure 2c) of 6665, 6800, and 6965 $Å^2$, which are smaller than the NMR structure by 10%, 8%, and 6%, respectively. Our smaller, more compact MD structure may result from the fact that explicit solvent was not

dx.doi.org/10.1021/jp306473u | J. Phys. Chem. B 2012, 116, 12159–12167

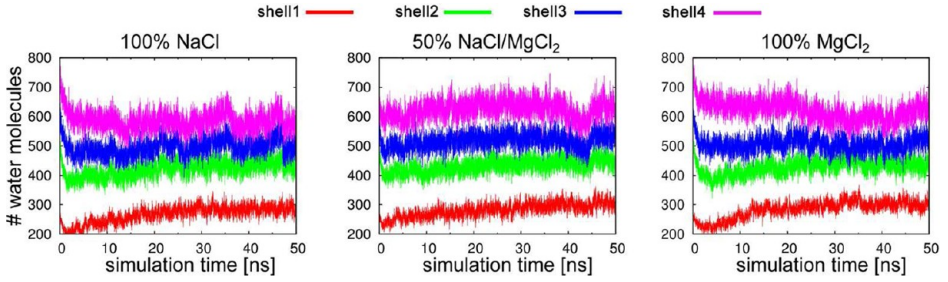

Figure 3. Time evolution of the occupancies of waters in the first (red), second (green), third (blue), and fourth (purple) hydration shells during MD simulations in (a) 100% NaCl, (b) 50% NaCl/$MgCl_2$, and (c) 100% $MgCl_2$, respectively. Convergence is observed after ~25 ns.

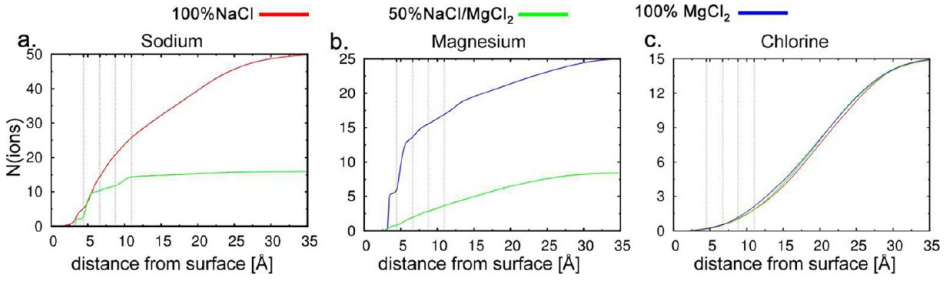

Figure 4. Ionic population analysis. Average number of (a) Na^+, (b) Mg^{2+}, and (c) Cl^- ions as a function of distance from the TWJ1 surface (PO_4^{2-}) in the pure NaCl (red), 50% NaCl/$MgCl_2$ (green), and pure $MgCl_2$ (blue) simulations. The water shells (as determined from the PO_4^{2-}–water distribution function [Figure S3]) are indicated in dashed vertical lines: shell 1, 0–4.5 Å; shell 2, 4.6–6.6 Å; shell 3, 6.7–8.8 Å; shell 4, 8.9–11.0 Å; bulk, >11.1 Å. Only snapshots of the MD simulation after 25 ns (i.e., after equilibration) were considered.

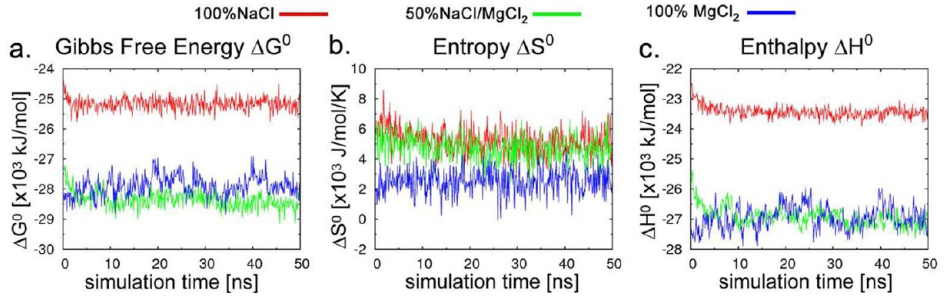

Figure 5. Time evolution of TWJ1 thermodynamic parameters. (a) Gibbs free energy ΔG^0, (b) entropy ΔS^0, and (c) enthalpy ΔH^0 for each of the three system considered in this study. The color scheme is similar to that in Figure 3. The thermodynamic observables are referenced to the solvent box, and so represent the free energy cost of solvating the vacuum TWJ1. Note, however, that the vacuum TWJ1 energies are not used as a reference and not needed when comparing the system as we reference the 50% NaCl/$MgCl_2$ and pure $MgCl_2$ energies in Table 1 to that of pure NaCl. Convergences in the thermodynamics occur within 25 ns of dynamics.

used when refining the NMR structures. To test this speculation, we minimized all 26 NMR structures with explicit water and salt and found minor decreases in the Rgyr of 0.5 ± 0.3 Å, far smaller than the reductions stated above. This may indicate that the NMR structures are trapped in local minima on the potential energy surface and would require finite temperature dynamics in order to find the lower energy, more compact conformations.

Equilibration of the DNA parameters usually occurs within a few nanoseconds; however, the convergence of the ion distributions may range from 0.1 to 0.5 μs.[49,50] A test of ion convergence is the population of ions within the "Manning radius" of 9 Å. After 25 ns of NPT dynamics, we find convergence of the ion populations to 0.60 ± 0.11 (pure NaCl), 0.66 ± 0.74 (50% $MgCl_2$), and 0.89 ± 1.0 (pure $MgCl_2$) (Figure S1), comparable to expected 0.78 from counterion condensation theory and validating our annealing procedure. Our results are also in general agreement with the computational results of Savelyev and Papoian[51] who found fractions of 0.65–0.73 for Na^+ ions around B-DNA helices.

3.2. Structure of the First and Second Hydration Shells. We first checked for any differences in hydration level of our simulated TWJ1 compared to regular B-DNA helices. Indeed experimental gel electrophoresis and circular dichroism spectroscopy studies by Muhuri et al.[52] showed that TWJs are less hydrated than corresponding double helices, and this difference in hydration is directly related to their increased thermal stability. To perform such an analysis, each water molecule was assigned a value of first, second, third, fourth, or bulk based on their distance from the DNA surface: <4.5, 4.5–6.7, 6.8–8.8, 8.9–11.0, and >11.1 Å, respectively (Figure S3). We find that TWJ1 is over 50% less hydrated than a representative set of DNA double helices. From Figure 3 and Table S2, we calculate a water surface density of 0.0426, 0.0435, and 0.0432 molecules/Å^2 for the pure NaCl, 50% $MgCl_2$, and pure $MgCl_2$, respectively, compared to 0.0875 molecules/Å^2 for 10 random sequenced, 18 base-pair B-DNA double helices.

dx.doi.org/10.1021/jp306473u | J. Phys. Chem. B 2012, 116, 12159–12167

Table 2. Relative Free Energy $\Delta\Delta G$ (kJ/mol), Enthalpy $\Delta\Delta H$ (kJ/mol), and Entropy $\Delta\Delta S$ (J/mol/K) of the Hydration Shells and DNA of the 50% NaCl/$MgCl_2$ and 100% $MgCl_2$ Simulation Relative to the 100% NaCl Simulation[a]

	50% NaCl/$MgCl_2$			100% $MgCl_2$		
	$\Delta\Delta G$	$\Delta\Delta H$	$\Delta\Delta S$	$\Delta\Delta G$	$\Delta\Delta H$	$\Delta\Delta S$
shell1	−503.4	−584.2	−230.4	−1040.6	−1213.9	−577.3
shell2	−552.7	−451.3	411.7	−1009.1	−721.6	968.6
shell3	−37.9	−55.7	−19.4	−90.8	−121.3	−121.6
shell4	−13.4	−33.4	−21.7	−30.4	−36.9	−43.4
DNA	−1774.2	−1752.0	−66.4	753.8	664.1	−304.7

[a]The hydration shell water energies are first referenced to that of the bulk waters in the same simulation and then to corresponding shells in the 100% NaCl simulation. Statistics were collected during the last 25 ns of the 50 ns MD trajectory, with uncertainties less than 0.5%.

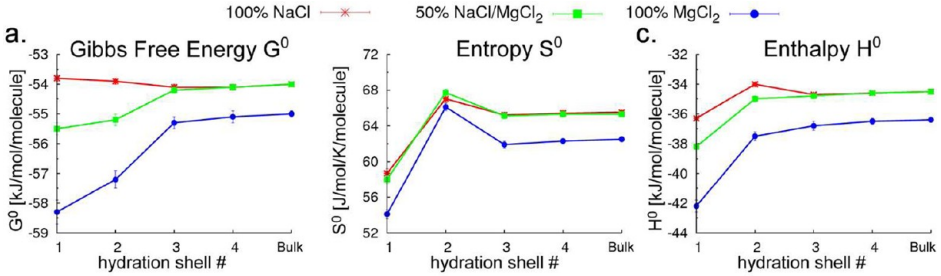

Figure 6. Hydration shell thermodynamics of TWJ1. Thermodynamics of simulations with pure NaCl (red stars), 50% NaCl/$MgCl_2$ (green squares), and pure $MgCl_2$ (blue circles) are obtained by averaging over the last 25 ns of the 50 ns MD simulation. The hydration shells distances are the same as defined in Figure 3. The absolute (a) free energy G^0, (b) entropy S^0, and (c) enthalpy H^0 all have errors smaller than the symbols except where noted. Mg^{2+} acts to stabilize the first and second hydration shells enthalpically. There is a compensation reduction in entropy of the first hydration shell. The second hydration shell has anomalously high entropy, however, and represents a frustrated layer sandwiched between the relative immobilized first and bulklike third layers.

Second, we checked the distribution of the ions around the TWJ1 surface by the ion−PO_4^{2-} distance distribution profiles (Figure 4). We find that the first hydration shell contains the same number of Mg^{2+} as Na^+ ions so that the normalized occupancy (number of ions times charge) of Mg^{2+} is twice that of Na^+. It has been well established that divalent cation will preferentially condense on the negatively charged DNA backbone due to increased electrostatic interactions, so this result is not surprising. Indeed, Bai et al. used buffer equilibration and atomic emission spectroscopy to show a threefold increase in the Mg^{2+} concentration around a DNA molecule compared to Na^+, even in solutions with Na^+ in fourfold excess.[53] Interestingly, due to the excess salt in our simulations, we find that the population of ions in the second hydration shell is greater than in the first: while the second shell is approximately 30% larger than the first, it has increased ion population by 70%, 65%, and 14% for the pure NaCl, 50% $MgCl_2$, and pure $MgCl_2$ systems, respectively.

3.3. Effect of Ions on System Stability. The temporal evolution of the absolute free energy (G^0), entropy (S^0), and enthalpy (H^0) is shown in Figure 5. In general, we find that the free energy (Figure 5a) decreases initially and then fluctuates about the mean after approximately 15 ns for the pure NaCl and 50% $MgCl_2$ systems, respectively, and slightly longer for the 100% $MgCl_2$ system. This correlates with the convergence of the structural parameters shown previously, indicating that the 2PT method provides enough resolution to distinguish individual structural motifs during dynamics.

Further insights can be gleaned by separately considering the enthalpic and entropic contributions to the free energy of the DNA, water shells, and ions. Such analysis allows for the straightforward determination of the solvation free energy ΔG_{solv}, i.e., the free energy change in bringing an isolated TWJ1 molecule with free energy G_{DNA} from the gas phase into the solvent of ionic strength C_T with free energy $G_{solvent}$:

$$\begin{aligned}\Delta G_{solv} &= G_{tot} - (G_{DNA}^{vacuum} + G_{solvent}) + R \ln C_T \\ &= (G_{DNA}^{solution} + G_{water}^{solution} + G_{ions}^{solution}) \\ &\quad - (G_{DNA}^{vacuum} + G_{solvent}) + R \ln C_T \end{aligned} \quad (1)$$

To circumvent the need to define an external reference state, we estimate the relative stabilities of the 50% and pure $MgCl_2$ systems (ΔG_A) relative to pure NaCl (ΔG_B):

$$\Delta\Delta G_{AB} = \Delta G_A - \Delta G_B = \Delta G_{DNA}^{AB} + \Delta(\Delta G_{water} + \Delta G_{ions}) \quad (2)$$

ΔG_{water} and ΔG_{ions} are the stabilities of the ions and water in the various hydration shells relative to the bulk, which can be evaluated from the same simulation provided that the thermodynamic functions are converged. ΔG_{ions} is negligible, as shown in Tables S2, and can be ignored.

Consider first the relative stability of the 50% $MgCl_2$ system. We find that this system is 11.5% more stable than the pure NaCl system, arising from a 12.9% gain in enthalpy that overcompensates for a 3.1% loss of entropy (Table 2). A little less than 2/3 of the increased system stability arises from more favorable electrostatic interactions of larger, less compact DNA molecule with the condensed Mg^{2+} ions, consistent with the predictions of continuum elastic theory, where the formation of a delocalized cloud shields negative phosphate charges.[54] These Mg^{2+} ions also stabilize the hydration waters enthalpically, which overcomes a 15% loss of entropy and accounts for the remaining 4.5% net gain in total free energy.

On the other hand, in the pure $MgCl_2$ system increased condensation of the Mg^{2+} ions on the TWJ1 backbone leads to

dx.doi.org/10.1021/jp306473u | J. Phys. Chem. B 2012, 116, 12159−12167

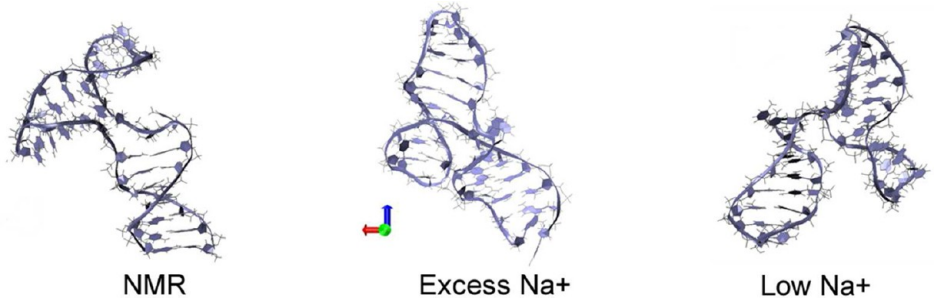

Figure 7. Comparison of the starting NMR TWJ1 structure, the average MD structure in 0.1 M excess NaCl, and an alternate structure in no excess NaCl (low Na^+). The alternate structure in low Na^+ is the thermodynamically stable conformer after ~60 ns of dynamics.

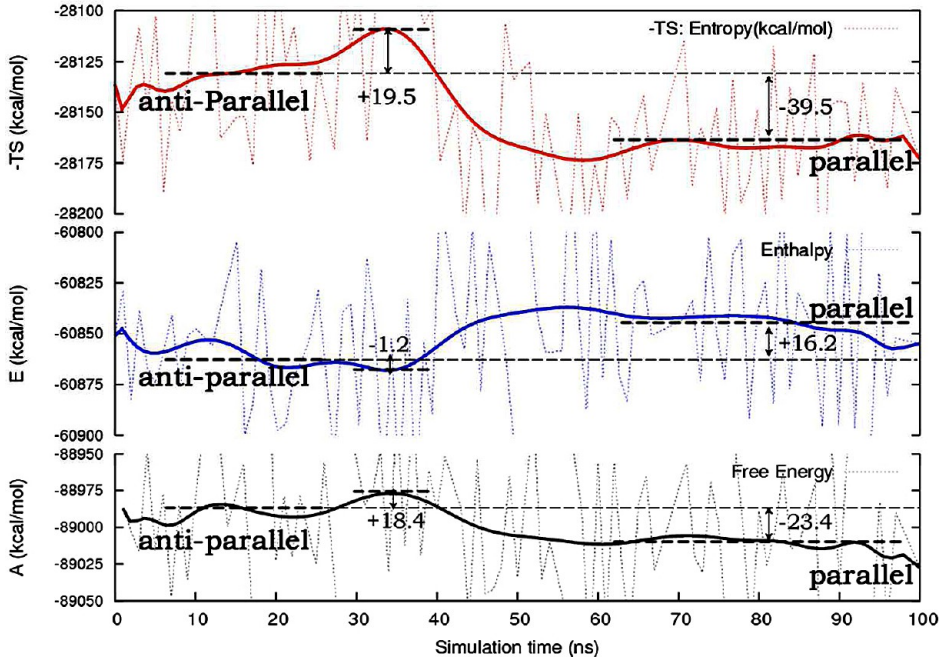

Figure 8. Thermodynamics profile of TWJ1 in Na^+ (low salt) at 300 K during 100 ns of dynamics. The total entropy (TS: red) and enthalpy (including zero-point energy corrections: blue) are indicated, and the Helmholtz free energy (black) is obtained from the sum. The data (dashed lines) are averaged and smoothened by a Bezier function (solid lines). The averaged energies have fluctuations of ±5 kcal/mol, identical to those in bulk water with the same system size, and represent the fluctuations for a finite system. The more compact achiral conformer (averaged from 60 to 100 ns) is 23 kcal/mol more stable than the chiral (starting NMR) conformer (averaged from 10 to 30 ns), due to a 40 kcal/mol increase in the total entropy and a 16 kcal/mol decrease in enthalpy. The barrier for the transition is calculated to be 18 and 42 kcal/mol for the forward and reverse transitions, respectively.

significant distortion of the DNA base-pair interactions and a more irregular structure.[15] The TWJ1 molecule is thus thermodynamically 3% less stable than in pure NaCl. Conversely, the free energy of the water molecules is greatly increased due to favorable electrostatic interactions with the magnesium ions, leading to a net increase in the total free energy of 2.3%. We underscore that the free energy gain in pure $MgCl_2$ does not arise from reduced DNA repulsion from condensed Mg^{2+}, but rather from enthalpic stabilization of the hydration shell waters. Indeed the hydration waters and DNA in pure $MgCl_2$ lose considerable entropy. Further, our results might provide an explanation for the measured increase and then eventual decrease in DNA melting temperature[55] with increasing Mg^{2+} concentration.

3.4. Thermodynamic Character of Hydration Shells. Having established that the thermodynamics of the hydration shells contribute to, and in some cases determine, the total system stability, we separately considered the free energy, entropy, and enthalpy of the individual hydration shells. As shown in Figure 6, the free energy profile is relatively flat in pure NaCl although the entropy and enthalpy show opposite compensatory trends. For example, the first solvation shell gains ~2 kJ/mol in enthalpy but loses ~7 e.u. of entropy (1 e.u. = 1 J/mol/K) in the first hydration shell, resulting in the same free energy as the bulk, within the confidence limit of our calculations (±0.1 kJ/mol). Generally, the entropy and enthalpy of the water shells in pure NaCl converge to the bulk value after the second hydration shell.

In contrast, systems containing $MgCl_2$ generally show first shell with increased stability and nearly monotonic decreases to the bulk, with convergence after the fourth hydration shell. We find it illuminating to more carefully consider the effects of Mg^{2+} on the thermodynamics of the first hydration shell, as these water molecules are most strongly perturbed by the divalent cation and therefore may contain the thermodynamic signature of overall solvation. Overall, the ~7.5 e.u. loss in

dx.doi.org/10.1021/jp306473u | J. Phys. Chem. B 2012, 116, 12159−12167

entropy is overcompensated by a 3.8 and 5.8 kJ/mol gain in enthalpy in the 50% and pure $MgCl_2$ systems, respectively, resulting in net free energy gains of −1.5 and −3.3 kJ/mol, respectively. We note that these interfacial waters comprise but a small fraction (<15%) of the total number of waters in our simulation shell yet account for half the increased water stability, underscoring their prominence in DNA solvation with Mg^{2+}.

While the first hydration shell may be the most prominent in thermodynamically stabilizing TWJ1 in $MgCl_2$, the second hydration shell displays the most peculiar entropic character. As noted previously, we measure an unusually high concentration of the divalent cation in this second shell. The presence of these ions can well be expected to reduce the entropy of the second shell waters as was evident for the first shell. Yet, we find that the entropy of this second shell is greatly enhanced over even the bulk, with increases of 1.5, 1.8, and 3.6 e.u. for the pure NaCl, 50% $MgCl_2$, and pure $MgCl_2$ systems, respectively. This suggests an entropically frustrated second hydration shell of water molecules, sandwiched between a relatively immobile first shell and a bulklike third shell. These second shell waters have enhanced molecular librational entropy (Table S3), i.e., faster rotations and enhanced low frequency rattling motions (as in a solid). The effect is more pronounced in Mg^{2+} due to increased ordering of the first shell. Indeed, in the case of pure $MgCl_2$, the increased entropy of the second shell means that this shell contributes 40−45% of the total water free energy gain in the system, while the third and fourth hydration shells contribute <10%.

3.5. Effect of Sodium Salt Concentration. In our above simulations, we added excess 0.1 M salt to our system to mimic the experimental conditions. In contrast, a common approach of simulations of biological systems is to add just sufficient Na^+ or Cl^- to achieve charge neutrality. To check the consequences of ionic strength, we also performed extensive (100 ns) simulations with no excess salt; i.e., we added 35 Na^+ ions to our TWJ1 structure in order to neutralize the DNA backbone charge.

Indeed, we find very dramatic differences in the low salt simulations, leading to results in pronounced disagreement with experiments. As shown in Figure 7, these low salt simulations lead to stabilization of structures with chirality (stacking angle on arms A and B on arm C) opposite that of experiment and opposite that from our simulation using physiological salt conditions. Structural analysis indicates that this low salt conformer is 5% smaller and has 2% less surface waters than the TWJ1 in excess NaCl. Thus dehydration is the thermodynamic driving force for the low salt structure.

Free energy analysis indicates that the low salt conformer is −92 kJ/mol more stable than the high salt structure (figure 8), due primarily to the gain in entropy upon releasing 16 water molecules from the surface, where they are 5 kJ/mol/molecule less stable, into the bulk. Similarly, Savelyev and Papoian[56] used a very simple model and estimated an entropy gain of 3.35 kJ/mol/molecule for release of water from the first solvation shell. Thus the stability of the interfacial waters increases with increasing Na^+ ionic concentration, as was demonstrated previously for Mg^{2+}. The converse is also true: lower ionic strengths destabilize the hydration shells relative to the bulk, producing a thermodynamic driving force for dehydration of the DNA molecule. These results quantify the finding of Cheatman,[50] who showed that the structure and dynamics of nucleic acids are affected by the solvent environment, specifically the concentration of the ions. Based on these results, we strongly recommend that simulations of proteins and nucleic acids and other macromolecules be carried out with salt concentrations mimicking that of the experimental systems.

3.6. Feasibility of Thermodynamic Calculations of Biomolecules in Explicit Salt. Finally, we note that the 2PT analysis allows an interpretation of the dynamical transition in terms of the enthalpic and entropic components (Figure 8). Here we see that the transition from the NMR (parallel) to the low salt (antiparallel) structure is dominated by the increase in entropy (due to the dehydration of the TWJ and release of water into the solvent). This leads to a thermodynamic barrier of 77 kJ/mol of which $-T\triangle S$ contributes 81.8 kJ/mol. We note that this thermodynamic analysis involves a system with 26 185 atoms and requires insignificant additional computations beyond the MD. Such calculations would be impractical for standard thermodynamic integration techniques.

4. CONCLUSIONS AND SCOPE

We have presented a structural and thermodynamic analysis of a simple branched DNA junction under various salt concentrations. The interpretations of these simulations were facilitated by the efficient 2PT method, where reliable thermodynamics of individual microstates of the system can be obtained from as little as 20 ps of simulations. A further advantage of this method is that it allows the calculation of these thermodynamic properties dynamically along a regular MD trajectory, meaning that structural and phase transition can now be routinely quantified. The major finding of this study is that the first and second hydration shell contributes significantly to the stabilization of TWJ1 in the presence of Mg^{2+}. The first shell waters are highly ordered and effectively immobilized. In dramatic contrast, the second shell is highly disordered and has the highest entropy.

While our thermodynamic analysis shows marked difference in the thermodynamic character of the hydration shell waters in the presence of the divalent ion, some care needs to be exercised when interpreting these results. As in all such studies, the fidelity of the results can depend dramatically on the quality of the force field employed, although some care was employed to use the most up-to-date DNA and ion parameters. Nevertheless, Mg^{2+} ions are notoriously difficult to model, owing to the formal +2 charge which severely immobilizes its hydration shell water molecules.[57] Additionally, the fact that the force fields employed in this study are not polarizable and therefore do not facilitate charge transfer between the ions and the DNA is another potential limitation.

The latter point deserves more elaboration. The physics of DNA−ion transfer has been shown to be appreciable for guanine rich DNA molecules with divalent cations.[58] Petrov et al.[59] have estimated a charge transfer of 0.1 e^- between the guanines nucleoside and Mg^{2+}, which over the observed first shell distance of 4.5 Å represent a small (5%) difference in that particular electrostatic interaction. Further, the experimental p*K*a of Mg^{2+} in water is 11.4[60] (ionic strength, $I = 0$), and 12.2−12.8 ($I > 0$). This means that Mg^{2+} will be a dominant species at medium pH and up to pH = 11.4. We therefore believe that $Mg(H_2O)_6^{2+}$ is a reasonable model for the cation near the TWJ1 surface and any effects due to the charge transfer between the DNA and Mg^{2+} ion are negligible and can be ignored.

Finally, we note that the thermodynamic observables converge to the bulk in NaCl by the second solvation shell,

but not until the fourth shell in the case of $MgCl_2$, or some 1 nm away from the DNA surface. Thus the long-range effect of Mg^{2+}, which is twice that of Na^+, may have implications in the molecular recognition of these motifs. We also highlight the importance of mimicking the experimental salt concentrations in MD simulations, since simulations in very low salt led to a structure of the opposite chirality to experiment being preferentially stabilized.

■ ASSOCIATED CONTENT

Supporting Information

Figures S1−S3, Tables S1−S4, and methods detailing the 2PT method. This material is available free of charge via the Internet at http://pubs.acs.org.

■ AUTHOR INFORMATION

Corresponding Author

*E-mail: tpascal@wag.caltech.edu (T.A.P.); wag@wag.caltech.edu (W.A.G.). Phone: 626-395-2731. Fax: 626-585-0918.

Author Contributions

The manuscript was written through contributions of all authors. All authors have given approval to the final version of the manuscript.

Notes

The authors declare no competing financial interest.

‖A C++ code implementing the 2PT method and compatible with most standard compilers is available upon request from the authors: tpascal@wag.caltech.edu (T.A.P.) or wag@wag.caltech.edu (W.A.G.).

■ ACKNOWLEDGMENTS

The authors thank Dr. Mario Blanco, Prof. Ned Seeman, Jim Canary, and Eric Winfree for useful discussions. Partial support for this work was from the U.S. National Science Foundation (grants CTS-0608889 and CTS- 0548774). The MSC computational facilities were provided by ARO-DURIP and ONR-DURIP. Additional computing resources were provided by a generous allocation from the KISTI supercomputing facility.

■ REFERENCES

(1) Kitts, P. A.; Nash, H. A. *Nature* **1987**, *329*, 346.
(2) Sinden, R. R. *Nature* **2001**, *411*, 757.
(3) Cleary, J. D.; Nichol, K.; Wang, Y. H.; Pearson, C. E. *Nat. Genet.* **2002**, *31*, 37.
(4) Seeman, N. C. *DNA Cell Biol.* **1991**, *10*, 475.
(5) Shen, Z. Y.; Yan, H.; Wang, T.; Seeman, N. C. *J. Am. Chem. Soc.* **2004**, *126*, 1666.
(6) van Buuren, B. N. M.; Overmars, F. J. J.; Ippel, J. H.; Altona, C.; Wijmenga, S. S. *J. Mol. Biol.* **2000**, *304*, 371.
(7) Warner, R. C.; Fishel, R. A.; Wheeler, F. C. *Cold Spring Harbor Symp. Quant. Biol.* **1978**, *43*, 957.
(8) McKinney, S. A.; Declais, A. C.; Lilley, D. M. J.; Ha, T. *Nat. Struct. Biol.* **2003**, *10*, 93.
(9) Welch, J. B.; Walter, F.; Lilley, D. M. J. *J. Mol. Biol.* **1995**, *251*, 507.
(10) Record, M. T.; Anderson, C. F.; Lohman, T. M. *Q. Rev. Biophys.* **1978**, *11*, 103.
(11) Chandler, D. *Nature* **2005**, *437*, 640.
(12) Pal, S. K.; Zhao, L. A.; Zewail, A. H. *Proc. Natl. Acad. Sci. U.S.A.* **2003**, *100*, 8113.
(13) Auffinger, P.; Hashem, Y. *Curr. Opin. Struct. Biol.* **2007**, *17*, 325.
(14) Cheatham, T. E.; Kollman, P. A. *J. Mol. Biol.* **1996**, *259*, 434.
(15) Maiti, P. K.; Pascal, T. A.; Goddard, W. A., III. *J. Nanosci. Nanotechnol.* **2007**, *7*, 1712.
(16) Maiti, P. K.; Pascal, T. A.; Vaidehi, N.; Heo, J.; Goddard, W. A., III. *Biophys. J.* **2006**, *90*, 1463.
(17) Maiti, P. K.; Pascal, T. A.; Vaidehi, N.; Goddard, W. A. *Nucleic Acids Res.* **2004**, *32*, 6047.
(18) Kollman, P. *Chem. Rev.* **1993**, *93*, 2395.
(19) Rothemund, P. W. K. *Nature* **2006**, *440*, 297.
(20) Yan, H.; Zhang, X. P.; Shen, Z. Y.; Seeman, N. C. *Nature* **2002**, *415*, 62.
(21) Maune, H. T.; Han, S.-p.; Barish, R. D.; Bockrath, M.; Goddard, W. A., III; Rothemund, P. W.; Winfree, E. *Nat. Nanotechnol.* **2010**, *5*, 61.
(22) Lin, S. T.; Maiti, P. K.; Goddard, W. A. *J. Phys. Chem. B* **2010**, *114*, 8191.
(23) Lin, S. T.; Blanco, M.; Goddard, W. A. *J. Chem. Phys.* **2003**, *119*, 11792.
(24) Altona, C. *J. Mol. Biol.* **1996**, *263*, 568.
(25) Lilley, D. M. J.; Clegg, R. M. *Q. Rev. Biophys.* **1993**, *26*, 131.
(26) Bernstein, F. C.; Koetzle, T. F.; Williams, G. J. B.; Meyer, E. F.; Brice, M. D.; Rodgers, J. R.; Kennard, O.; Shimanouchi, T.; Tasumi, M. *J. Mol. Biol.* **1977**, *112*, 535.
(27) Holst, M.; Saied, F. *J. Comput. Chem.* **1993**, *14*, 105.
(28) Perez, A.; Marchan, I.; Svozil, D.; Sponer, J.; Cheatham, T. E.; Laughton, C. A.; Orozco, M. *Biophys. J.* **2007**, *92*, 3817.
(29) Berendsen, H. J. C.; Grigera, J. R.; Straatsma, T. P. *J. Phys. Chem.* **1987**, *91*, 6269.
(30) Aqvist, J. *J. Phys. Chem. B* **1990**, *94*, 8021.
(31) Joung, I. S.; Cheatham, T. E. *J. Phys. Chem. B* **2008**, *112*, 9020.
(32) Plimpton, S. *J. Comput. Phys.* **1995**, *117*, 1.
(33) Pascal, T. A.; Abrol, R.; Mittal, R.; Wang, Y.; Prasadarao, N. V.; Goddard, W. A., III. *J. Biol. Chem.* **2010**, *285*, 37753.
(34) Plimpton, S. J.; Pollock, R.; Stevens, M. Particle-Mesh Ewald and rRESPA for Parallel Molecular Dynamics Simulations; *Proceedings of the Eighth SIAM Conference on Parallel Processing for Scientific Computing*, Minneapolis, MN, 1997.
(35) Shrake, A.; Rupley, J. A. *J. Mol. Biol.* **1973**, *79*, 351.
(36) Eyring, H.; Ree, T. *Proc. Natl. Acad. Sci.* **1961**, *47*, 526.
(37) Lin, S. T.; Jang, S. S.; Cagin, T.; Goddard, W. A. *J. Phys. Chem. B* **2004**, *108*, 10041.
(38) Pascal, T. A.; Lin, S. T.; Goddard, W. A., III. *Phys. Chem. Chem. Phys.* **2011**, *13*, 169.
(39) Huang, S.-N.; Pascal, T. A.; Goddard, W. A.; Maiti, P. K.; Lin, S.-T. *J. Chem. Theory Comput.* **2011**, *7*, 1893.
(40) Lin, S. T.; Maiti, P. K.; Goddard, W. A. *J. Phys. Chem. B* **2005**, *109*, 8663.
(41) Li, Y. Y.; Lin, S. T.; Goddard, W. A. *J. Am. Chem. Soc.* **2004**, *126*, 1872.
(42) Pascal, T. A.; Lin, S.-T.; Goddard, W.; Jung, Y. *J. Phys. Chem. Lett.* **2012**, *3*, 294.
(43) Pascal, T. A.; He, Y.; Jiang, S.; Goddard, W. A. *J. Phys. Chem. Lett.* **2011**, *2*, 1757.
(44) Jang, S. S.; Lin, S. T.; Maiti, P. K.; Blanco, M.; Goddard, W. A.; Shuler, P.; Tang, Y. C. *J. Phys. Chem. B* **2004**, *108*, 12130.
(45) Jana, B.; Pal, S.; Maiti, P. K.; Lin, S. T.; Hynes, J. T.; Bagchi, B. *J. Phys. Chem. B* **2006**, *110*, 19611.
(46) Pascal, T. A.; Goddard, W. A.; Jung, Y. *Proc. Natl. Acad. Sci. U.S.A.* **2011**, *108*, 11794.
(47) Kumar, H.; Mukherjee, B.; Lin, S.-T.; Dasgupta, C.; Sood, A. K.; Maiti, P. K. *J. Chem. Phys.* **2011**, *134*, 124105.
(48) Spanu, L.; Donadio, D.; Hohl, D.; Schwegler, E.; Galli, G. *Proc. Natl. Acad. Sci.* **2011**, *108*, 6843.
(49) Ponomarev, S. Y.; Thayer, K. M.; Beveridge, D. L. *Proc. Natl. Acad. Sci. U.S.A.* **2004**, *101*, 14771.
(50) Cheatham, T. E. *Curr. Opin. Struct. Biol.* **2004**, *14*, 360.
(51) Savelyev, A.; Papoian, G. A. *J. Am. Chem. Soc.* **2006**, *128*, 14506.
(52) Muhuri, S.; Mimura, K.; Miyoshi, D.; Sugimoto, N. *J. Am. Chem. Soc.* **2009**, *131*, 9268.

(53) Bai, Y.; Greenfeld, M.; Travers, K. J.; Chu, V. B.; Lipfert, J.; Doniach, S.; Herschlag, D. *J. Am. Chem. Soc.* **2007**, *129*, 14981.
(54) Mohanty, U.; Spasic, A.; Kim, H. D.; Chu, S. *J. Phys. Chem. B* **2005**, *109*, 21369.
(55) Ott, G. S.; Ziegler, R.; Bauer, W. R. *Biochemistry* **1975**, *14*, 3431.
(56) Savelyev, A.; Papoian, G. A. *J. Phys. Chem. B* **2008**, *112*, 9135.
(57) Ohtaki, H. *Monatsh. Chem. Chem. Monthly* **2001**, *132*, 1237.
(58) Petrova, P.; Koca, J.; Imberty, A. *Eur. J. Biochem.* **2001**, *268*, 5365.
(59) Petrov, A. S.; Lamm, G.; Pack, G. R. *J. Phys. Chem. B* **2002**, *106*, 3294.
(60) Burgess, J. *Metal Ions in Solution*; Ellis Horwood, distributed by Halsted Press: Chichester; New York, 1978.